

All-Optical Dissipative Discrete Time Crystals

Hossein Taheri,^{1,*} Andrey B. Matsko,² Lute Maleki,³ and Krzysztof Sacha⁴

¹*Department of Electrical and Computer Engineering,
University of California Riverside, 3401 Watkins Drive, Riverside, CA 92521*

²*Jet Propulsion Laboratory, California Institute of Technology,
4800 Oak Grove Drive, Pasadena, California 91109-8099, USA*

³*OEwaves Inc., 465 North Halstead Street, Suite 140, Pasadena, CA, 91107, USA*

⁴*Instytut Fizyki Teoretycznej, Uniwersytet Jagielloński,
ulica Profesora Stanisława Łojasiewicza 11, PL-30-348 Kraków, Poland*

Time crystals are periodic states exhibiting spontaneous symmetry breaking in either time-independent or periodically forced quantum many-body systems. Spontaneous modification of *discrete* time translation symmetry in a periodically driven physical system can create a discrete time crystal (DTC). DTCs constitute a state of matter with properties such as temporal rigid long-range order and coherence which are inherently desirable for quantum computing and quantum information processing. Despite their appeal, experimental demonstrations of DTCs are scarce and hence many significant aspects of their behavior remain unexplored. Here, we report the experimental observation and theoretical investigation of photonic DTCs in a Kerr-nonlinear optical microcavity. Empowered by the simultaneous self-injection locking of two independent lasers with arbitrarily large frequency separation to two cavity modes and a dissipative soliton, this room-temperature all-optical platform enables observing novel states like DTCs carrying defects, and realizing long-awaited phenomena such as DTC phase transitions and mutual interactions. To the best of our knowledge, this is the first experimental demonstration of a dissipative DTC, as well as the concurrent self-injection locking of two continuous-wave lasers to different modes of the same family in a Kerr cavity. Combined with monolithic fabrication, it can result in chip-scale DTCs, paving the way for liberating time crystals from sophisticated laboratory setups and propelling them toward real-world applications.

Symmetry is a central concept and unifying theme of physics. In quantum mechanics, stationary solutions of the Schrödinger equation must follow the symmetries of the system Hamiltonian. A many-body system, however, may fail to obey these symmetries. The formation of ordinary spatial crystals constitutes a well-known example in which a periodic distribution of atoms prevails even though space translation symmetry in the governing theory does not favor any particular location in the system [1]. This epitomizes spontaneous symmetry breaking (SSB), perhaps the most significant aspect of the universal notion of symmetry which appears in various branches ranging from condensed matter physics to the standard model of electroweak interactions [2]. At the same time, while for centuries physicists treated space and time on different footings, Einstein underscored their shared relative nature and combined them into *space-time*. In 2012, Frank Wilczek wondered if this similitude could be extended by searching for a temporal analogue for the SSB of ordered atoms in crystalline solids [3]. This quest flamed a heated scientific debate [4–7], kindled much excitement, and gave rise to a prolific area of research centered around what is now considered a new phase of matter, *time crystals* (TCs).

While the original search for TCs targeted continuous time translation symmetry (TTS) in non-driven quantum systems [3], it was soon realized that intriguing aspects of temporal SSB can rather be observed in periodically driven, so-called Floquet, non-equilibrium systems. An

isolated many-body quantum system driven by a periodic external force may spontaneously assume a stable state evolving with a period different from that of the drive [8–10]. A *discrete* time crystal (DTC) emerges when the period of the system response is an integer multiple of the drive period. DTCs now lie at the focus of intense research, with various time crystalline states, such as fractional DTCs and quasi-crystals, proposed and yet waiting to be observed in experiments; see [11–13] and references therein. In isolated translationally invariant Floquet systems, interactions and disorder can suppress driving-induced thermalization to create infinitely long-lived DTCs. Furthermore, exponentially long-lived DTCs can arise in such systems in the absence of disorder when the external forcing frequency is much larger than the system’s local energy scales. Understanding ergodicity breaking mechanisms in DTCs is another avenue of current active research [14].

Closed systems, while a significant stepping stone, do not capture the full potential of TCs. In fact, the study of DTCs in *dissipative* open quantum systems is highly germane and immensely important, especially when TC applications, e.g., for quantum memory and computation, are concerned. Dissipation can heat up driven isolated quantum many-body systems and destroy time crystallinity. Yet, coupling to an external environment drains energy from a driven system and a periodic steady state can prevail [15–17]. Only recently has the investigation of dissipative DTCs gained traction [18–26].

We report in this work the experimental demonstration and theoretical study of all-optical, room-temperature, quantum DTCs in Kerr-nonlinear microresonators. This demonstration relies on the simultaneous self-injection locking of two independent continuous-wave (CW) pump lasers with arbitrary multi-FSR (free spectral range) frequency separation to two same-family cavity modes and a dissipative optical soliton. A DTC is realized when the periodicity of the soliton pulse train becomes an integer multiple of the drive period defined by the beating of the pumps through robust subharmonic generation. The existence of patent discrete TTS and its spontaneous breaking via the emergence of discrete symmetry with a larger integer-multiple period distinguishes DTC formation in our system from subharmonic entrainment [27, 28]. Compared to a recent theoretical proposal for continuous-time SSB and boundary TCs in coupled Kerr cavities [29], our work demonstrates discrete-time SSB, and moreover in a significantly simpler experimental setup constituting one resonator. We observe different m -tupling DTCs in which the integer m (the response-to-drive period ratio) can be chosen much larger than 2, hence readily realizing recently-predicted so-called *big* DTCs [30–33]. We present a thorough analysis, emphasizing that DTC size m and its state can be tuned by frequency tuning of the external laser pumps, and illustrating that these photonic DTCs possess temporal long-range order and can be realized robustly over a range of system parameters. We explore possible extensions to new states such as defective DTCs, the temporal counterpart of solid-state crystals with point defects (i.e., vacancies, dislocations, and interstitials) [34]. Our results inaugurate an ideal photonic platform to experimentally demonstrate a whole set of time crystalline phenomena which not only have remained inaccessible in hitherto explored systems, but some have not even been deemed possible thus far. This novel platform will empower future theoretical and experimental investigations of long-sought DTC properties such as phase transitions, and support applications demanding coherence and precision like quantum computation and timekeeping. Combined with the highly developed monolithic fabrication of optical high-Q (quality factor) microresonators, our proposed system can lead to the demonstration of compact low-phase-noise photonic frequency dividers as well as chip-scale DTCs, not only creating unprecedented opportunities for further exploration of the physics of TCs, but also paving the way for liberating them from complex laboratories and adopting TCs in real applications.

RESULTS

Concept. Many-body Hamiltonian of a bosonic system can possess spatial or temporal translation symmetry which may be spontaneously broken if bosons interact

sufficiently strongly. Formation of optical or matter-wave solitons—robust solitary waves preserving their shape upon propagation—in systems of photons or massive particles exhibits a prominent example studied theoretically and experimentally over the past few decades [35–43]. These symmetry-broken states represent stable solutions which can accurately be described through mean-field models.

In ultra-cold atomic ensembles, if inter-atomic interactions are attractive and sufficiently strong, it becomes energetically favorable for the atoms to group into a single localized wave-packet evolving along a classical orbit with a period that is an integer multiple of the external drive periodicity [13]. Such a Bose-Einstein condensate (BEC) breaks the discrete TTS, thereby realizing a DTC. In the optical platform utilized here, a localized photon wave-packet (a self-synchronized dissipative optical soliton) arises from the nonlinear interaction of photons in the Kerr resonator [44, 45]. While a monochromatically pumped Kerr microcomb does not define a discrete TTS (see the *Supplementary Information*), two energetic pumps with judiciously chosen power and frequency can excite subharmonics and hence break the discrete symmetry defined by their beatnote. Specifically, the simultaneous driving of a high-Q Kerr-nonlinear resonator at two different frequencies f_{P_1} and f_{P_2} primarily creates a periodic pattern (henceforth called the modulated background waveform) rotating around the cavity, whose periodicity is dictated by the spectral spacing between the two pump frequencies. For two pumps separated by M FSRs of the resonator (M being an integer), the periodicity is given by $T = 1/(f_{P_2} - f_{P_1}) = T_R/M$, where $T_R = L/v_g$ is the round-trip time of the cavity, L denotes the resonator circumference and v_g the group velocity at the relevant frequency range. The modulated background creates a potential grid in the resonator and acts as a *rotating lattice trap* for optical solitons. For a certain region in the power vs. pump-resonance detuning plane for the driving lasers, the system can spontaneously generate one or multiple solitons per cavity round-trip time which will reside on top of the background pattern, trapped in the potential array. The periodicity of the resulting pulse train will in general differ from that of the modulated background and effective driving field (T), giving rise to discrete temporal SSB. Depending on the number of soliton peaks per cavity round-trip time and their distribution with respect to the modulated background, the periodicity of the generated pulse train will be mT , where $1 \leq m \leq M$ is an integer. Period multiplication and DTC formation occurs for $m > 1$.

Were we interested in spatial crystals, we would inquire about the periodicity of the system in space at a fixed moment of time, i.e., the moment of detection. We are, however, interested in temporal crystalline structures and should therefore exchange the roles of space and time to observe the TTS described above and its spontaneous

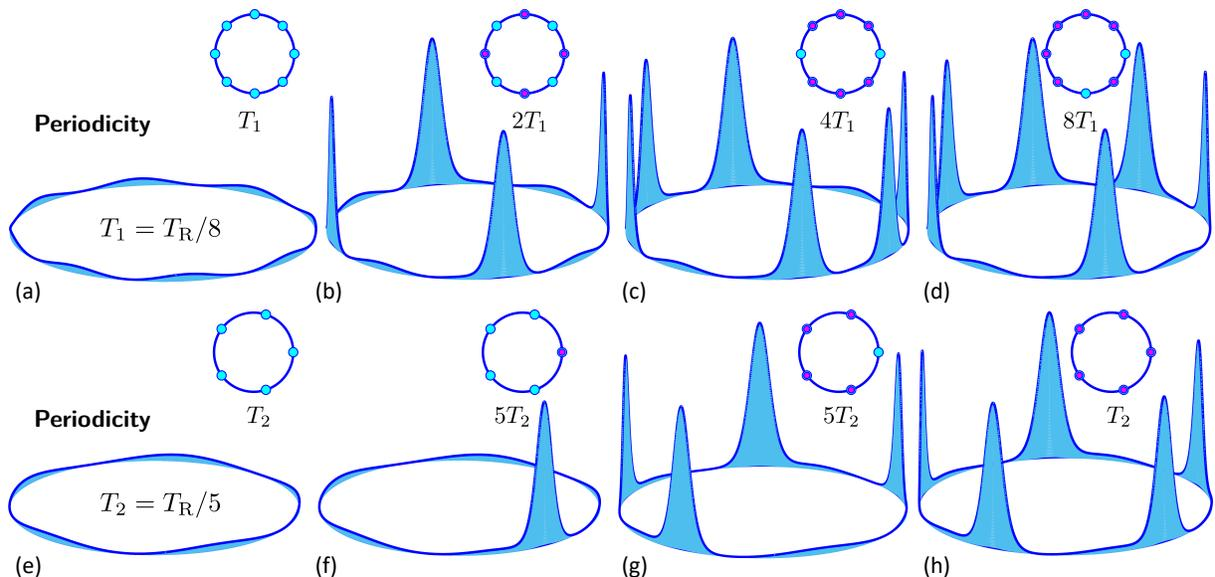


FIG. 1. Symmetry breaking, period multiplication, and DTC formation in an optical resonator pumped by two lasers separated by (a-d) $M = 8$ and (e-h) $M = 5$ cavity FSRs. (a, e) The beating between the two pumps modulates the background waveform and creates a rotating lattice trap near the resonator periphery, where optical modes are localized. (a) For $M = 8$ the temporal periodicity of the lattice trap is $T_1 = T_R/8$. (b) Spontaneous formation of a soliton in every second well of the lattice potential breaks the discrete TTS giving rise to a period-doubling DTC (periodicity $2T_1$). (c) When a trapped soliton is missing in every fourth potential well, a period-quadrupling DTC (with period $4T_1$) is formed. (d) If the distribution of multiple solitons in the lattice does not possess any certain symmetry, a period-octupling DTC (with periodicity $8T_1$) will be created. Here, 6 solitons are asymmetrically trapped around the lattice. (e) Lattice periodicity is $T_2 = T_R/5$ for $M = 5$. Symmetry considerations reduce the variety of observable DTCs in this case. When only one soliton is trapped in the potential lattice (f), or when all but one of the potential wells host a soliton (g), a period-quintupling DTC is formed (periodicity $5T_2$), while if one soliton is trapped in each potential well, discrete TTS will not be broken (h). Insets illustrate top-view schematics with an empty circle (cyan) for each lattice trap and a filled circle (magenta) denoting a soliton.

breaking. We choose a spatial point in the path of the photons (i.e., the location of an imaginary detector) and observe whether the probability of the detector clicking (counting photons) evolves periodically with time [13]. Two examples illustrating the two different cases of even and odd integer M (i.e., $M = 8$ and $M = 5$ FSR spacing between the pumps with periodicity $T_1 = T_R/8$ and $T_2 = T_R/5$, respectively) are shown in Fig. 1. Here we look at the collective photon waveform in a co-rotating reference frame in a ring-shaped resonator, which can be accurately modeled using a variant of the nonlinear Schrödinger equation (NLSE), including detuning, damping, and two-pump driving; see the Methods Section. The potential lattice created by the beating of the pumps is shown in Figs. 1(a) and (e). For $M = 8$, if a soliton is spontaneously formed in every second well of the lattice potential, as in Fig. 1(b), discrete TTS will be broken such that the system evolves with period $2T_1$, giving rise to a period-doubling DTC. If, however, a trapped soliton is missing from every fourth well, then SSB forms a period-quadrupling DTCs (i.e., period $4T_1$); Fig. 1(c). Finally, if only one soliton per round-trip spins around the resonator, or if the positioning of multiple solitons in the periodic lattice does not possess any symme-

try, the pattern should traverse a full circle to resume its original shape and a period-octupling DTC, one evolving with periodicity $8T_1$, will be created; see Fig. 1(d) for an example depicting 6 solitons asymmetrically distributed around the resonator circumference. We note that if one soliton is trapped in each of the potential wells, then discrete TTS will not be violated. In this case, when the system is observed in the laboratory frame (e.g., as the pulse train couples out of the microresonator), a soliton arrives every subsequent driving period T_1 at a given point in space.

For $M = 5$ too, when one soliton is trapped in each potential well, discrete-time SSB will not occur; [Fig.1(h)]. Symmetry considerations, however, reduce the variety of observable DTCs in this case. If only one soliton is trapped in the modulated background potential lattice [Fig.1(f)], or if all but one of the potential wells host a soliton [Fig.1(g)], then TTS will be spontaneously broken and a period-quintupling DTC will be formed (periodicity $5T_2$). Different ratios of the response to drive periodicity, and hence realizations of discrete TTS breaking, can be envisioned for other pump separations. For instance, if solitons sit in every third periodic lattice site in a resonator driven by two pumps spectrally spaced by

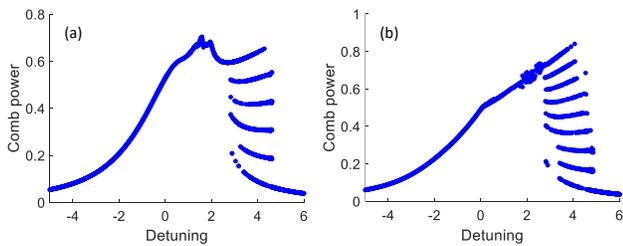


FIG. 2. Comb power versus detuning curves for (a) 5-FSR and (b) 8-FSR separation between the two pumps, when laser powers are kept fixed. Each data point corresponds to one numerical integration of the governing equations from a random initial waveform till a steady state (for non-chaotic states) prevailed. Spontaneous soliton formation occurs in step-like regions to the right of the curves. Dispersion parameter matching the experimental resonator ($D_2 = 2\pi \times 6.8$ kHz) was used. The horizontal axis shows the normalized detuning of the stronger pump ($-\sigma_1/\kappa$), for fixed detuning difference between the lasers ($\sigma_2 = \sigma_1 + D_2 M^2/4$); see Methods. In (a) normalized pump powers were (1.4, 0.9), and in (b) they were (1.5, 0.99).

$M = 9$ FSRs, then a period-tripling DTC will be realized. Indeed the DTC platform introduced here can readily accommodate m -tupling DTCs with $m \gg 1$, creating so-called *big* DTCs with dramatic SSB [33].

We should emphasize that DTCs can be formed in a microresonator driven by two pumps over a range of laser frequencies and powers. Figures 2(a, b) show steady-state pulse train power vs. pump-resonance detuning, respectively, for $M = 5$ and $M = 8$, where the horizontal axis is the detuning of the stronger pump normalized to the resonator half-width at half-maximum (HWHM) linewidth while the vertical axis is the normalized intracavity power. Each data point in Fig. 2 indicates one simulation run till steady states, for non-chaotic microcombs, prevailed. Here, the step-like multi-stability region on the right of each curve denotes where discrete TTS breaking occurs, the lowest branch corresponding to the modulated background [cf. Figs. 1(a, e)]. It is seen that in each case, the number of step-like branches (disregarding the lowest step) equals M , because the two pumps separated by M FSRs discretize the resonator circumference (i.e., each round-trip time) and create preferable residing lattice sites for the spontaneously formed solitons. Each step pertains to a constant number of solitons per round-trip time, starting from 1 (the branch right above the lowest) and ending with M , the top-most branch. As remarked earlier, depending on the positioning of the solitons with respect to the background lattice, a different m -tupling DTC will be realized.

The introduced DTCs are robust with respect to system parameters and possess temporal long-range order. We have verified that all of the various TTS breaking states depicted in Fig. 1 are stable over hundreds of cavity photon lifetimes (thousands of the driving period, and

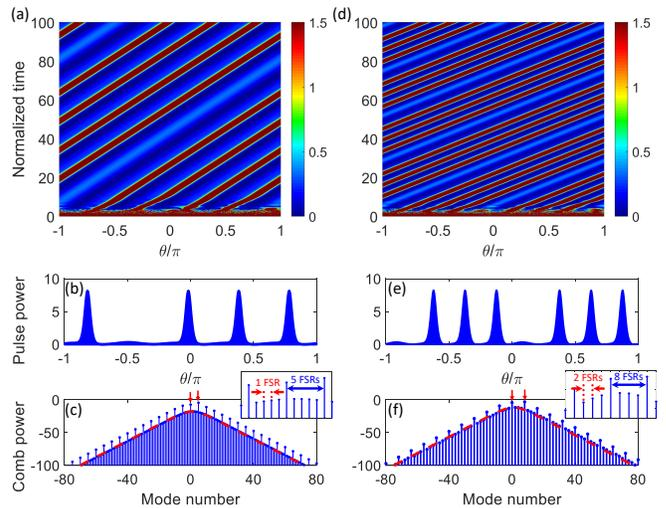


FIG. 3. Representative numerical integration results demonstrating temporal long-range order in two of the states in Fig. 1. Left panels (a-c) correspond to Fig. 1(g), and right panels (d-f) to Fig. 1(c). (a, d) Temporal evolution of pulse trains over 100 normalized times (200 cavity photon lifetimes and thousands of the driving period). Pulses are initialized through hard excitation, the horizontal axis is the angle around the resonator, and the vertical axis is the evolution time. Dark red lines denote soliton trajectories. (b, e) Snapshots of the pulse trains at the end of the integration time in (a, d). (c, f) Frequency spectra (logarithmic scale) of the DTC states plotted in (b, e). Each spectrum is centered on one of the pumped modes labeled 0, and the horizontal axis shows frequency normalized to the resonator FSR. Vertical red arrows mark the pumps and red dashed curves show hyperbolic secant envelopes. Insets are zoomed-in spectra around the center, showing the beatnote of the pumps (blue) and the separation of adjacent subharmonics (red). Generation of multiple subharmonics between the pumps is manifest. Numerical parameters match those of Fig. 2, with $-\sigma_1/\kappa = 4$.

much longer than the lifetime of DTCs demonstrated in initial experiments [46, 47]). Two examples are depicted in Figs. 3(a, d); cf. Figs. 1(g, c). Figures 3(b, e) show snapshots of the pulse trains at the end of the integration time in Figs. 3(a, d), respectively. The horizontal axis in panels (a, b, d, e) is θ , the azimuthal angle around the circular resonator, which is related to the fast time τ through $\theta = 2\pi\tau/T_R$; see the Methods Section. The tilted trajectory of the soliton peaks moving upward in Figs. 3(a, d) depends on the frequency separation between the pumps and their detuning from respective resonances, as well as a slight soliton center frequency shift (recoil) resulting from the presence of the second pump [48]. This tilt amounts to a fixed-speed rotation around the resonator and can be removed with a change in the angular velocity of the co-moving reference frame.

Before presenting experimental results, we note that periodic pulse trains correspond to frequency combs in the conjugate Fourier domain, i.e., an equidistant array

of frequency tones spaced by the repetition rate $1/T_R$ [49]. The frequency comb spectra of the DTC states of Figs. 3(b, e) are plotted in Figs. 3(c, f). The horizontal axis shows frequency normalized to the resonator FSR, and the spectrum is centered on one of the pumped mode frequencies labeled 0. The red arrows mark the pumps and the red dashed lines show hyperbolic secant (sech) soliton envelopes in Figs. 3(c, f). Multiple frequency tones are seen to be generated between the two pump harmonics in both representative examples. This *subharmonic* generation in the frequency domain accompanies periodic multiplication in the time domain which was discussed earlier and is a signature of DTCs.

Experiments. For the experimental demonstration of the photonic DTCs introduced above, we utilized a high-Q whispering gallery mode (WGM) magnesium fluoride (MgF_2) crystalline resonator of 1.06 mm radius (32.8 GHz FSR), pumped by two prism-coupled lasers. The setup schematic is illustrated in Fig. 4(a); see the Methods Section for further information on resonator preparation, pulse train generation, and measurements. The radio frequency (RF) signal of the output-coupled optical wave was demodulated on a fast photodiode to ensure the coherent nature of the generated pulse train. For the two pumps not generating any subharmonics (i.e., the modulated background with no solitons trapped in the potential lattice), a narrow RF signal is generated; see the blue curve in Fig. 4(b). We observed that the generation of subharmonics (solitons riding the background), further reduces the phase noise, narrowing the RF signal peak as a result of the stronger mutual coupling between frequency harmonics. One example is plotted by the red curve in Fig. 4(b).

Two representative spectra corresponding to SSB and DTC formation are plotted in Figs. 4(c, f), respectively for $M = 4$ and $M = 3$ FSRs separating the driving lasers. The pumps are marked by red arrows and the red dashed curves show hyperbolic secant envelopes. The stronger pump was kept nearly at 1545 nm in both cases. The matching numerical modeling spectra are depicted to the right of the experimental data, in Figs. 4(d, g); excellent agreement between experiment and theory is observed. The corresponding time-domain pulse trains per round-trip time are shown on the far right, in panels (e, h) of Fig. 4, with snapshots of the pulse trains revolving around the resonator circumference as insets. From the insets, it is obvious that Figs. 4(c-e) represent a period-quadrupling DTC while Figs. 4(f-h) demonstrate a period-tripling DTC.

In our experiment, we have observed multi-stability similar to what is depicted in Fig. 2, where each middle branch corresponds to a different DTC realization; see also Figs. S3(c) and S4 (blue curves) in the *Supplementary Information*. These multi-stable states consisted of (1) four-wave mixing (FWM) of the two pumps creating harmonics separated by their beatnote [as in Fig.

S1(b), with the corresponding RF beatnote plotted in blue in Fig. 4(b)], and (2) subharmonic generation between the pumps, which correspond to DTC formation [as in Figs. 4(c, f), with RF beatnote plotted in red in Fig. 4(b)]. Note that different subharmonic arrays translate into different pulse numbers per round-trip time. After finding the appropriate parameter regime for subharmonic generation in our experiments, we always observed one of the states (1) or (2) in every subsequent run. In particular, in every realization of subharmonics between the two pumps, we observed the same envelope and a narrow RF beatnote, hinting at the stable nature of the realized DTC states.

DISCUSSION

A periodically forced dissipative many-body system qualifying as a DTC meets certain criteria. First, it possesses discrete TTS, evident from the time-dependence of its equation of motion. However, steady states (i.e., steady-state solutions of the equation of motion) evolving with a cycle that is an integer multiple of the period dictated by the drive can emerge spontaneously in the system. Second, the symmetry-broken steady states emerge without relying on fine tuning and are stable over a range of parameters. Third, the many-body system is in the thermodynamic limit and the symmetry-broken states can be accurately described by a mean-field approach. Subharmonic generation in the dichromatically pumped Kerr microcavity system introduced in this work qualifies as a dissipative DTC because it meets all of the said criteria. The two pumps define a discrete TTS in the system, manifest in the equations of motion (detailed in Methods), which is broken by the realization of certain periodic steady states of the system. These states, accompanied by subharmonic generation, demonstrate SSB at integer response to drive periodicity ratios. The subharmonics in symmetry-broken states emerge robustly, both in numerical modeling and experiments, with various (e.g., 2-, 3-, and 4-FSR) frequency separations of the pumps and possess temporal long-range order; see also *Supplementary Information* Section V. Finally, the DTCs are in the thermodynamic limit of infinitely many photons and are well captured by a mean-field model (the modified LLE, see Methods).

Besides the DTC states introduced thus far, it is possible to create a *nearly perfect* m -tupling DTC with a missing, dislocated, or extra soliton spoiling crystalline symmetry. Such defective DTCs mirror spatial crystal defects such as vacancies, dislocations, and interstitials in condense matter physics [34]. Panels (a, d) in Fig. 5 depict two examples. In (a), one soliton is missing from a period-doubling DTC while in (d) a soliton is dislocated by one lattice site [cf. Fig. 1(b)]. The location of the missing or misplaced soliton (with respect to the perfect

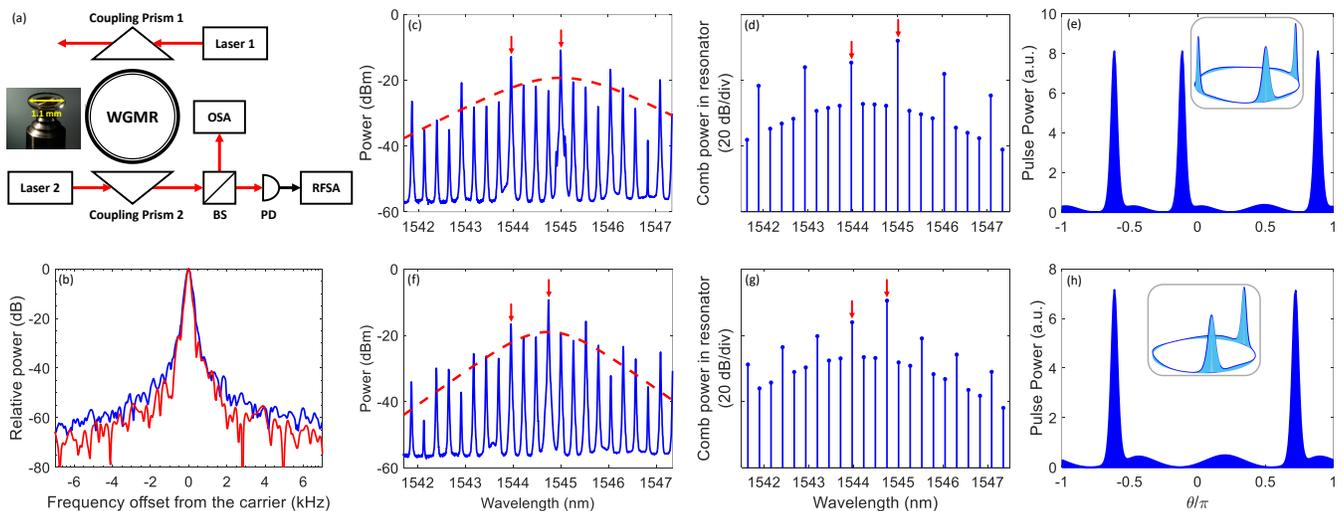


FIG. 4. Experimental observation of all-optical DTCs. (a) Experimental setup; WGMR: Resonator, OSA: Optical spectrum analyser, RFSA: Radio frequency spectrum analyser, BS: Beam splitter, PD: Photodetector. (b) RF signal ensuring stable pulse train generation. For the two pumps not generating any subharmonics (modulated background with no trapped solitons), a narrow RF signal is generated (blue, 32.8 GHz carrier frequency). The generation of solitons trapped in the background lattice further narrows the RF signal peak. An example is the red curve (10.9 GHz carrier frequency), corresponding to the experimental spectrum plotted in (f). (c, f) Spectra corresponding, respectively, to period-quadrupling ($M = 4$) and period-tripling ($M = 3$) DTCs. Pumps are marked by red arrows, and red dashed curves show soliton envelopes. The stronger pump was at 1545 nm in (c) and 1544.8 nm in (f). (d, g) Numerical modeling spectra matching (c, f). (e, h) Time-domain pulse trains per round-trip time (numerical), with snapshots of pulses revolving around the resonator circumference as insets.

DTC) in each case is indicated by a red arrow in the top-view ring schematic appearing in the top left corner. The bottom panels (b, e) and (c, f) in Fig. 5 plot, respectively, snapshots of the optical pulse train per round-trip time (again, the red arrows hinting at the position of the missing or dislocated soliton) and their corresponding power spectra. In Figs. 5(d, e), a dotted arrow connects the current position of the dislocated soliton to its placement in the perfect crystal. The sech-shaped envelop of the frequency spectra in Fig. 5(c) is the same as that shown in Fig. 3(f) and is not redrawn here. If an extra soliton is spontaneously formed in any of the unoccupied lattice sites in Fig. 1(b), a DTC with interstitial defect will be formed. It is worth noting that each of these pulse trains has a unique frequency (Fourier) spectrum and can be identified unambiguously in the frequency domain. Moreover, the appearance of DTCs carrying defects is more conspicuous and consequential in big TCs (for $1 \ll m < M$) and Fig. 5 is intended to clearly illustrate the phenomenon. Finally, we should emphasize that the analogy drawn here between defects in DTCs and those in solid state spatial crystals is, strictly speaking, not exact because in the latter the spontaneous breaking of continuous, rather than discrete, TTS occurs.

The DTC platform introduced here is closely related to microresonator-based Kerr frequency combs (Kerr microcombs) [44]. While many aspects of soliton microcomb formation have been explored over the past decade, our novel pumping scheme combines dichromatic driv-

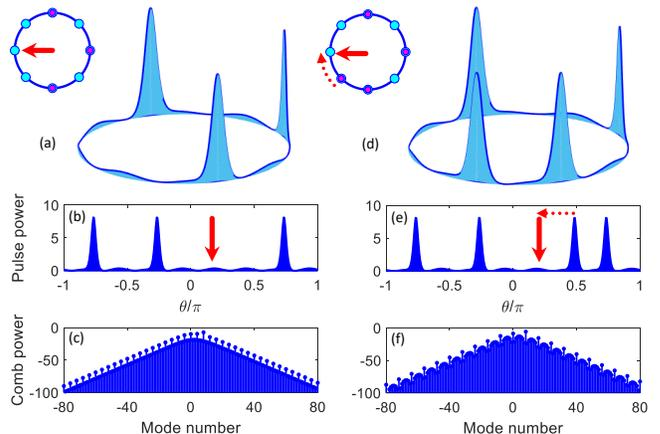


FIG. 5. Examples of DTCs carrying defects. A point defect (vacancy) in which one soliton is missing from a period-doubling DTC (a), and dislocation in which one soliton is misplaced by one lattice site (d); cf. Fig. 1(b). The location of the missing or misplaced soliton (with respect to the perfect DTC) in each case is indicated by a red arrow in the top-view ring schematic (insets). (b, e) Snapshots of the optical pulse train per round-trip time, matching the top panels (a, d), respectively, with red arrows hinting at the position of the missing or dislocated soliton. (c, f) Power spectra corresponding to (b, e). Dotted arrows in (d, e) connect the current position of the dislocated soliton to its placement in the perfect crystal. Numerical parameters are the same as those in Fig. 3(d-f).

ing and soliton self-injection locking, thereby effectuating turnkey soliton formation in the presence of clear discrete TTS. Driving a high-Q Kerr resonator with a CW laser pump can break *continuous* TTS symmetry by generating a soliton pulse train [50]. Cherenkov dispersive wave (DW) emission in the presence of higher-order dispersion (HOD) or avoided mode crossing (AMC) will modulate the background [51–53], and trap pulse peaks in so-called soliton crystals [48, 54]. However, as detailed in the *Supplementary Information*, resonator HOD and AMC do not establish any discrete TTS and, accordingly, monochromatically-pump resonators cannot host DTCs.

As described earlier, when, instead of one, two CW pumps (or another temporally structured pump wave) drive the resonator, solitons will be trapped in the potential introduced through the background modulation [48, 55–57]. In our dichromatically-pumped microresonator, the cavity is engineered to ensure higher-order dispersion and mode anti-crossings do not interfere with soliton formation in the proximity of the pumps. Additionally, *both* driving lasers coherently lock to two resonator modes and a spontaneously-formed soliton microcomb [48, 58]. The physics of the hyperparametric process resulting in stable subharmonic generation in this platform guarantees the division of the pumps’ beatnote to equal subharmonics (integer response to drive periodicity ratio) and hence elegantly allows for confirming DTC behavior through standard frequency-domain measurements without resorting to complex temporal techniques [28, 59]; single-shot pulse measurement methods can facilitate further investigations into the rigidity of photonic DTCs. Independent of the resonator geometry, these phenomena are expected to occur also in integrated ring and fiber-ferrule Fabry-Pérot resonators [57]. We speculate that DTCs can similarly be observed even in other resonator or mode-locked laser types such as fiber cavities [60, 61] or harmonically mode-locked lasers; in the latter case, certain frequency pinning mechanisms for ensuring robust pulse dropout are necessary. It is worth emphasizing that dual-microcomb spectroscopy setups, in contrast to our experiments, rely on two very close pump frequencies (typically different by less than 1% of an FSR) each creating its own microcomb; see [44] and Refs. [36–40] therein. Furthermore, addition of a second pump (or sideband) frequency to improve thermal stabilization does not lock the second frequency to the microcomb and merely adds extra power inside the cavity [62].

In light of recent advancements in integrated nonlinear and quantum photonics [44, 63, 64], the variety of emerging material platforms [53], and the flexibility offered by advanced dispersion engineering, revolutionary progress in the study of TCs is possible using the platform introduced in this work. Exploiting the plethora of experimental techniques and commercial equipment available to photonics for the investigation of the various

aspects of TCs will prove crucial. For instance, utilizing delicate laser tuning [65] and synchronous pumping techniques [57] empowers the deterministic creation of target DTC states and exploring their interaction [66] in small experimental setups. Furthermore, building upon mode-locked laser pumping of fiber resonators [60], synchronous pumping can be used to drive solitons in larger microresonators. Generation of microcomb solitons with few-GHz range repetition rates is possible, and at these rates, efficient (i.e., with small half-wave voltage V_π) ultrafast electro-optic modulation combined with pulse shaping will furnish excellent flexibility for the controlled realization of various DTC phases and transitions between them [56, 57]. Most excitingly, with progress in the monolithic integration of lasers and optical modulators, small-footprint, room-temperature, all-optical DTC may soon become a reality.

Although still in their infancy, TCs are inspiring future technology, and ideas for their applications are crystallizing. New paradigms for overcoming coherence limitations in quantum systems involve transitioning to the driven out-of-equilibrium regime. Indeed, among the most anticipated properties of DTCs are their robustness and temporal long-range order which enable maintaining coherence much longer than is currently possible in equilibrium systems. From the perspective of Kerr microcomb technology, the dichromatic self-injection locking pumping scheme utilized here can be used for microwave photonic frequency division and multiplexing [58, 67]; the repetition rate is locked to the beatnote of the two pumps, resulting in characteristically different behavior compared to standard monochromatically driven combs. Furthermore, two-point locking of the pumps (for instance by pinning lasers externally to frequency references such as two atomic transitions) enables stabilizing even a narrow-band microcomb and can obviate the exacting requirement of octave-spanning spectral coverage which has so far been a holy grail of microcomb research. As such, precision microcomb-based metrology and timekeeping can be extended to uncharted frequency windows and new platforms in which material dispersion currently limits comb bandwidth and consequently $f-2f$ self-referencing [48]. Finally, recent studies [56, 68] have shown several technical advantages for seeding microcomb formation with a modulated pump. Yet, available modulator bandwidths do not allow generating sidebands multiple cavity FSRs away from the pump in a microresonator, especially in smaller diameters with hundreds of GHz to THz-level FSRs. Therefore, microcomb stabilization by two independent lasers constitutes a decisive step which brings the benefits of parametric seeding to small resonators, and further enhances the possibility of miniaturization, and reduced size, weight, and power consumption for future applications. In this work we have focused on a few FSRs separating the two pumps but suspect that the marriage of dichromatic pumping with self-injection

locking of both pumps to Kerr cavity modes of the same modal family involves very rich physics, warranting dedicated investigations, e.g., into the role of the beatnote of the pumps.

CONCLUSION

We have demonstrated, for the first time to the best of our knowledge, a versatile photonic platform utilizing two pump lasers concurrently self-injection-locked to different modes of a Kerr cavity, which exhibits spontaneous breaking of discrete TTS and dissipative DTC formation. Our two-pronged theoretical and experimental study shows that in a high-Q resonator driven at two frequencies, strongly interacting photons can spontaneously generate one or multiple temporal solitons, which crystallize in the rotating optical lattice formed by the beating between the pumps through robust subharmonic generation and can give rise to DTCs with various sizes (response-to-drive period ratios). Both theory and experiment verify that the generated DTCs possess temporal long-range order. Operating in room temperature, this platform lends itself to simplified investigations of unexplored time crystalline properties such as phase transitions and mutual interactions. Our results also demonstrate that integrated optics represents a robust and flexible platform for mimicking condensed matter physical systems. Paired with monolithic fabrication and well-developed techniques of quantum integrated photonics, this platform empowers fieldable chip-scale DTCs, thereby paving the path for extricating the time crystalline phase of matter from complex laboratory setups and employing them in real-world applications, e.g., in quantum computation and timekeeping.

METHODS

Equations and Numerical Modeling. Soliton formation, resulting in spontaneous symmetry breaking and DTC generation described in this work, can be accurately modeled using a variant of the NLSE, including detuning, damping, and driving, which is often referred to as the Lugiato-Lefever equation (LLE) [69]. Here we use an LLE variant modified for two-pump driving [48]. In the laboratory reference frame, this equation takes the form

$$\frac{\partial A}{\partial t} = \left(-\kappa - i\sigma_1 - ig|A|^2 - D_1 \frac{\partial}{\partial \theta} - i \frac{D_2}{2} \frac{\partial^2}{\partial \theta^2} \right) A + \mathcal{F}(\theta, t), \quad (1)$$

in which κ is the resonance half width at half maximum (HWHM), $\sigma_1 = 2\pi f_{P_1} - \omega_{j_0}$ represents the detuning of the first pump from its neighboring resonance ω_{j_0} , g is

the FWM gain, $D_1/2\pi = 1/T_R$ is the resonator FSR near the first pump, and $D_2 = \omega_{j_0+1} + \omega_{j_0-1} - 2\omega_{j_0}$ denotes the group velocity dispersion coefficient. Cavity resonant modes are labeled with integer eigenmode numbers j , and D_1 and D_2 (expressed in rad/s) are the first two coefficients in the Taylor series expansion of resonant mode frequencies ω_j in eigenmode number at the first pumped resonance ω_{j_0} , i.e., $\omega_j = \omega_{j_0} + D_1(j - j_0) + D_2(j - j_0)^2/2$; in the frequency range of interest, higher-order terms were negligibly small for the resonator utilized in our experiments. The variable t is the evolution time (sometimes referred to as the *slow* time), and θ is the azimuthal angle around the resonator, related to the *fast* time τ via $\theta = 2\pi\tau/T_R$ (modulo 2π). The intra-cavity field $A(\theta, t)$ is normalized such that $\int_{2\pi} d\theta |A(\theta, t)|^2/2\pi$ equals the total number of photons in the cavity at each time t . FWM gain is found from $g = n_2 c \hbar \omega_{j_0}^2 / (n_0^2 V_{j_0})$, where n_0 and n_2 are the linear and nonlinear indices of refraction, c is the vacuum speed of light, \hbar is the reduced Planck constant, and V_{j_0} is the effective nonlinear mode volume of the first pumped mode [53]. The drive term $\mathcal{F}(\theta, t)$ is given by

$$\mathcal{F}(\theta, t) = \sqrt{\kappa_{c_1}} \mathcal{F}_1 + \sqrt{\kappa_{c_2}} \mathcal{F}_2 e^{i[2\pi(f_{P_2} - f_{P_1})t - M\theta]}, \quad (2)$$

where M , as in the main text, is the number of FSRs separating the pump frequencies (i.e., $f_{P_2} - f_{P_1} = M/T_R$), $\kappa_{c_{1,2}}$ are the coupling coefficients to the two pumps, and $|\mathcal{F}_{1,2}|^2$ represent the rate of photons pumped by the lasers [48]. The beating between the two pumps appears in the exponent of the second driving term, where $M\theta = 2\pi(M/T_R)\tau = 2\pi(f_{P_2} - f_{P_1})\tau$.

Inspection of the drive term, Eq. 2, shows that Eq. 1 is periodic and invariant under transformations $t \rightarrow t + 1/(f_{P_2} - f_{P_1})$ and $\theta \rightarrow \theta + 2\pi/M$ [equivalently $\tau \rightarrow \tau + 1/(f_{P_2} - f_{P_1})$]. This periodicity defines the discrete time translation symmetry of the systems, which can be spontaneously broken by soliton formation in the resonator, as described in the main text.

Equation 1 can be simplified by transitioning to a reference frame rotating with angular velocity D_1 (i.e., $\theta \rightarrow \theta - D_1 t$, one round per T_R), rendering

$$\begin{aligned} \frac{\partial A}{\partial t} = & \left(-\kappa - i\sigma_1 - ig|A|^2 - i \frac{D_2}{2} \frac{\partial^2}{\partial \theta^2} \right) A \\ & + \sqrt{\kappa_{c_1}} \mathcal{F}_1 \\ & + \sqrt{\kappa_{c_2}} \mathcal{F}_2 \exp \{ i (\sigma_2 - \sigma_1 + D_2 M^2/2) t - iM\theta \}, \end{aligned} \quad (3)$$

in which σ_2 is the pump-resonance detuning of the second pump. For numerical integration, a non-dimensional form of Eq. 3 was found by normalizing time to twice the cavity photon lifetime (t/κ), detunings and dispersion coefficient to the HWHM ($-\sigma_{1,2}/\kappa$ and $-D_2/\kappa$), and intra-cavity waveform and pump powers to the sideband generation threshold $A_{th} = \sqrt{\kappa/g}$ in a monochromatically pumped cavity (A/A_{th} and $\sqrt{\kappa_{c_{1,2}}} \mathcal{F}_{1,2}/A_{th}$). We emphasize that the t -dependence on the right-hand side of Eq. 1

can be removed readily by a proper change of variables (e.g., $\theta \rightarrow \theta - 2\pi(f_{P_2} - f_{P_1})t/M$), yet the resulting equation will carry a $\partial A/\partial \theta$ term, further differentiating it from a damped, driven NLSE.

It is noteworthy that Eq. 1 can be derived from an equivalent set of nonlinear coupled-wave equations, each following the temporal evolution of one frequency comb harmonic, as detailed in Ref. [48]. Numerical modeling was performed using both the split-step Fourier transform (Eq. 3) and adaptive-step Runge-Kutta integration (couple-wave equations), with excellent agreement. To properly match experimental conditions, hard excitation with high-energy initial fields was utilized. In soft excitation of a cold cavity, the effect of vacuum fluctuations was incorporated through the addition of independent noise terms.

Resonator Preparation. The resonator was fabricated out of a magnesium fluoride (MgF_2) cylindrical preform by mechanical polishing. The preform rim was shaped into an oblate spheroid optimized for evanescent field coupling with a free space beam. Resonator radius was approximately 1.06 mm, while the radius of the vertical curvature was 0.2 mm. The resonator had an FSR of 32.8 GHz and loaded resonance bandwidth of approximately $2\kappa = 2\pi \times 200$ kHz. Resonance loaded bandwidth was tuned by adjusting the air gap between the coupling prisms and the resonator surface. The optical power emitted by the laser never exceeded 5 mW. Roughly 3 mW of power entered the resonator because of imperfect laser beam spatial structure and other non-idealities, indicating an insertion loss smaller than 3 dB. Resonator group velocity dispersion at the pumping frequency was $\beta_2 \simeq -4.9$ ps²/km, corresponding to $D_2 = 2\pi \times 6.8$ kHz. Formally, the normalized dispersion parameter D_2/κ impacts comb generation efficiency, so through modifying the coupling, we tuned the overall conversion efficiency.

Pulse Train Generation. To couple light in and out of the resonator, we utilized evanescent prism couplers made of BK7 glass. The coupling efficiency is better than 60%. The resonator generates microcombs corresponding to optical soliton trains (with hyperbolic secant spectral envelopes) if pumped with mW level optical power at around 1545 nm. The criteria for soliton pulse train generation constituted simultaneous observation of a stable sech-shaped frequency comb spectral envelope (on an OSA) as well as a low-noise radio frequency (RF) signal (on a fast photodiode) [67]. Microcomb repetition rate defines the frequency of the microwave signal. This measurement was performed using an RFSA, as shown in Fig. 4(a). High spectral purity of the RF signal indicates the high degree of coherence of the frequency comb.

When two lasers pump resonator modes, as shown in Fig. 4(a), generally harmonics at both laser frequencies, plus some sidebands are generated. When laser power exceeds a certain threshold and the frequency detuning is properly selected for both lasers, subharmonic generation

and a mode-locked frequency comb emerges [48, 55]. In both numerical modeling and experiments, the power of one laser was set above the threshold while the other had a power slightly below it. A coherent pulse train in this case was identified by an RF signal with smaller phase noise compared to the beat note of the two optical pumps directly demodulated on a photodiode; see Fig. 4(b).

Soliton Self-injection Locking. To generate a stable pulse train, one has to lock each laser to its neighboring resonator mode at an optimal frequency offset. We achieved this using the self-injection locking technique [58], in which no isolator is placed between each pump and the resonator, so the laser locks to a resonator mode when a small amount of light coupled to the mode scatters back toward the laser (resonant Rayleigh scattering). Through tuning the locking point by regulating the optical phase delay between the laser chip and the resonator, the frequency of one of the lasers was shifted to a spectral position where a microcomb was observed. DTC generation was then straightforward by selecting proper pump powers. To this end, we started from higher power levels, too high to sustain a microcomb. Laser currents were then reduced till stable subharmonic generation was observed. At this stage, the power of one pump was slightly above that required for initiating the hyperparametric process with a single laser while that of the other was below this threshold, and importantly neither pump could generate a soliton microcomb alone. One notable advantage of self-injection locking is simplified optical soliton generation in the cavity through soft excitation. In contrast, soliton microcomb generation without injection locking often relies on hard excitation or switching [50, 65]. It should be emphasized that the absence of anti-crossing-induced frequency pinning in the microcomb spectra confirms the negligible effect of avoided mode crossings in our experiments; see *Supplementary Information*, Section IV.

Note: During the submission of this work, a subsequent example of dissipative DTCs was reported in an atom-cavity system [70].

Data availability. The data that support the plots within this paper and other findings of this study are available from the corresponding author upon reasonable request.

Code availability. The codes used for this study are available from the corresponding author upon reasonable request.

* Corresponding author: hossein.taheri@ucr.edu

- [1] J. van Wezel and J. van den Brink, Spontaneous symmetry breaking in quantum mechanics, *Am. J. Phys.* **75**, 160401 (2007).
- [2] F. Strocchi, *Symmetry Breaking*, The Lecture Notes in Physics (Springer-Verlag, Berlin Heidelberg, 2005, 2008).

- [3] F. Wilczek, Quantum time crystals, *Phys. Rev. Lett.* **109**, 160401 (2012).
- [4] P. Bruno, Impossibility of spontaneously rotating time crystals: A no-go theorem, *Phys. Rev. Lett.* **111**, 070402 (2013).
- [5] H. Watanabe and M. Oshikawa, Absence of quantum time crystals, *Phys. Rev. Lett.* **114**, 251603 (2015).
- [6] A. Syrwid, J. Zakrzewski, and K. Sacha, Time crystal behavior of excited eigenstates, *Physical Review Letters* **119**, 250602 (2017).
- [7] V. K. Kozin and O. Kyriienko, Quantum time crystals from Hamiltonians with long-range interactions, *Phys. Rev. Lett.* **123**, 210602 (2019).
- [8] K. Sacha, Modeling spontaneous breaking of time-translation symmetry, *Phys. Rev. A* **91**, 033617 (2015).
- [9] V. Khemani, A. Lazarides, R. Moessner, and S. L. Sondhi, Phase structure of driven quantum systems, *Phys. Rev. Lett.* **116**, 250401 (2016).
- [10] D. V. Else, B. Bauer, and C. Nayak, Floquet time crystals, *Phys. Rev. Lett.* **117**, 090402 (2016).
- [11] K. Giergiel, A. Kuroś, and K. Sacha, Discrete time quasicrystals, *Phys. Rev. B* **99**, 220303 (2019).
- [12] L. Guo and P. Liang, Condensed matter physics in time crystals, *New Journal of Physics* **22**, 075003 (2020).
- [13] K. Sacha, *Time Crystals* (Springer International Publishing, 2020).
- [14] V. Khemani, R. Moessner, and S. L. Sondhi, A Brief History of Time Crystals, arXiv e-prints, arXiv:1910.10745 (2019).
- [15] G. Nicolis and I. Prigogine, *Self-organization in Nonequilibrium Systems* (John Wiley & Sons, New York, 1977).
- [16] H. Haken, *Synergetics – An Introduction*, 3rd ed. (Springer-Verlag, 1983).
- [17] P. Drummond, K. McNeil, and D. Walls, Non-equilibrium transitions in sub/second harmonic generation, *Optica Acta: International Journal of Optics* **27**, 321 (1980).
- [18] Z. Gong, R. Hamazaki, and M. Ueda, Discrete time-crystalline order in cavity and circuit QED systems, *Phys. Rev. Lett.* **120**, 040404 (2018).
- [19] F. Iemini, A. Russomanno, J. Keeling, M. Schirò, M. Dalmonte, and R. Fazio, Boundary time crystals, *Phys. Rev. Lett.* **121**, 035301 (2018).
- [20] F. M. Gambetta, F. Carollo, M. Marcuzzi, J. P. Garrahan, and I. Lesanovsky, Discrete time crystals in the absence of manifest symmetries or disorder in open quantum systems, *Phys. Rev. Lett.* **122**, 015701 (2019).
- [21] B. Buča, J. Tindall, and D. Jaksch, Complex coherent quantum many-body dynamics through dissipation, *Nature Communications* **10**, 1730 (2019).
- [22] H. Keßler, J. G. Cosme, M. Hemmerling, L. Mathey, and A. Hemmerich, Emergent limit cycles and time crystal dynamics in an atom-cavity system, *Phys. Rev. A* **99**, 053605 (2019).
- [23] J. G. Cosme, J. Skulte, and L. Mathey, Time crystals in a shaken atom-cavity system, *Phys. Rev. A* **100**, 053615 (2019).
- [24] H. Keßler, J. G. Cosme, C. Georges, L. Mathey, and A. Hemmerich, From a continuous to a discrete time crystal in a dissipative atom-cavity system, *New Journal of Physics* **22**, 085002 (2020).
- [25] A. Lazarides, S. Roy, F. Piazza, and R. Moessner, Time crystallinity in dissipative floquet systems, *Phys. Rev. Research* **2**, 022002 (2020).
- [26] J. O’Sullivan, O. Lunt, C. W. Zollitsch, M. L. W. Thewalt, J. J. L. Morton, and A. Pal, Signatures of discrete time crystalline order in dissipative spin ensembles, *New Journal of Physics* **22**, 085001 (2020).
- [27] D. C. Cole and S. B. Papp, Subharmonic Entrainment of Kerr Breather Solitons, *Physical Review Letters* **123**, 173904 (2019).
- [28] T. Xian, L. Zhan, W. Wang, and W. Zhang, Subharmonic Entrainment Breather Solitons in Ultrafast Lasers, *Physical Review Letters* **125**, 163901 (2020).
- [29] K. Seibold, R. Rota, and V. Savona, A dissipative time crystal in an asymmetric non-linear photonic dimer, *Physical Review A* **101**, 033839 (2020).
- [30] K. Giergiel, A. Kosior, P. Hannaford, and K. Sacha, Time crystals: Analysis of experimental conditions, *Phys. Rev. A* **98**, 013613 (2018).
- [31] F. M. Surace, A. Russomanno, M. Dalmonte, A. Silva, R. Fazio, and F. Iemini, Floquet time crystals in clock models, *Phys. Rev. B* **99**, 104303 (2019).
- [32] A. Pizzi, J. Knolle, and A. Nunnenkamp, Higher-order and fractional discrete time crystals in clean long-range interacting systems, *Nature Communications* **12**, 2341 (2021).
- [33] K. Giergiel, T. Tran, A. Zaheer, A. Singh, A. Sidorov, K. Sacha, and P. Hannaford, Creating big time crystals with ultracold atoms, *New Journal of Physics* **22**, 085004 (2020).
- [34] N. W. Ashcroft and N. D. Mermin, *Solid State Physics* (Holt-Saunders, 1976).
- [35] S. J. Carter, P. D. Drummond, M. D. Reid, and R. M. Shelby, Squeezing of quantum solitons, *Physical Review Letters* **58**, 1841 (1987).
- [36] Y. Lai and H. A. Haus, Quantum theory of solitons in optical fibers. i. time-dependent Hartree approximation, *Phys. Rev. A* **40**, 844 (1989).
- [37] S. R. Friberg, S. Machida, and Y. Yamamoto, Quantum-nondemolition measurement of the photon number of an optical soliton, *Physical Review Letters* **69**, 3165 (1992).
- [38] P. D. Drummond, R. M. Shelby, S. R. Friberg, and Y. Yamamoto, Quantum solitons in optical fibres, *Nature* **365**, 307 (1993).
- [39] Y. Castin, Bose-Einstein condensates in atomic gases: Simple theoretical results, in *Coherent atomic matter waves*, edited by R. Kaiser, C. Westbrook, and F. David (Springer Berlin Heidelberg, Berlin, Heidelberg, 2001).
- [40] J. Denschlag, J. E. Simsarian, D. L. Feder, C. W. Clark, L. A. Collins, J. Cubizolles, L. Deng, E. W. Hagley, K. Helmerson, W. P. Reinhardt, S. L. Rolston, B. I. Schneider, and W. D. Phillips, Generating solitons by phase engineering of a Bose-Einstein condensate, *Science* **287**, 97 (2000).
- [41] K. E. Strecker, G. B. Partridge, A. G. Truscott, and R. G. Hulet, Formation and propagation of matter-wave soliton trains, *Nature* **417**, 150 (2002).
- [42] L. Khaykovich, F. Schreck, G. Ferrari, T. Bourdel, J. Cubizolles, L. D. Carr, Y. Castin, and C. Salomon, Formation of a matter-wave bright soliton, *Science* **296**, 1290 (2002).
- [43] A. Syrwid and K. Sacha, Lieb-liniger model: Emergence of dark solitons in the course of measurements of particle positions, *Physical Review A* **92**, 032110 (2015).
- [44] T. J. Kippenberg, A. L. Gaeta, M. Lipson, and M. L. Gorodetsky, Dissipative Kerr solitons in optical microresonators, *Science* **361**, eaan8083 (2018).
- [45] H. Taheri, P. Del’Haye, A. A. Eftekhar, K. Wiesenfeld,

- and A. Adibi, Self-synchronization phenomena in the Lugiato-Lefever equation, *Physical Review A* **96**, 013828 (2017).
- [46] J. Zhang, P. W. Hess, A. Kyprianidis, P. Becker, A. Lee, J. Smith, G. Pagano, I.-D. Potirniche, A. C. Potter, A. Vishwanath, N. Y. Yao, and C. Monroe, Observation of a discrete time crystal, *Nature* **543**, 217 (2017).
- [47] S. Choi, J. Choi, R. Landig, G. Kucsko, H. Zhou, J. Isoya, F. Jelezko, S. Onoda, H. Sumiya, V. Khemani, C. von Keyserlingk, N. Y. Yao, E. Demler, and M. D. Lukin, Observation of discrete time-crystalline order in a disordered dipolar many-body system, *Nature* **543**, 221 (2017).
- [48] H. Taheri, A. Matsko, and L. Maleki, Optical lattice trap for Kerr solitons, *The European Physical Journal D* **71**, 153 (2017).
- [49] S. T. Cundiff, Phase stabilization of ultrashort optical pulses, *Journal of Physics D: Applied Physics* **35**, R43 (2002).
- [50] T. Herr, V. Brasch, J. Jost, C. Wang, N. Kondratiev, M. Gorodetsky, and T. Kippenberg, Temporal solitons in optical microresonators, *Nat. Photon.* **8**, 145 (2014).
- [51] V. Brasch, M. Geiselmann, T. Herr, G. Lihachev, M. H. P. Pfeiffer, M. L. Gorodetsky, and T. J. Kippenberg, Photonic chip-based optical frequency comb using soliton Cherenkov radiation, *Science* **351**, 357 (2016).
- [52] A. Matsko, W. Liang, A. Savchenkov, D. Eliyahu, and L. Maleki, Optical Cherenkov radiation in overmoded microresonators, *Optics Letters* **41**, 2907 (2016).
- [53] A. Kovach, D. Chen, J. He, H. Choi, A. H. Dogan, M. Ghasemkhani, H. Taheri, and A. M. Armani, Emerging material systems for integrated optical Kerr frequency combs, *Adv. Opt. Photon.* **12**, 135 (2020).
- [54] D. C. Cole, E. S. Lamb, P. Del'Haye, S. A. Diddams, and S. B. Papp, Soliton crystals in Kerr resonators, *Nature Photonics* **11**, 671 (2017).
- [55] T. Hansson and S. Wabnitz, Bichromatically pumped microresonator frequency combs, *Physical Review A* **90**, 013811 (2014).
- [56] H. Taheri, A. Eftekhari, K. Wiesenfeld, and A. Adibi, Soliton formation in whispering-gallery-mode resonators via input phase modulation, *IEEE Photonics J.* **7**, 1 (2015).
- [57] E. Obrzud, S. Lecomte, and T. Herr, Temporal solitons in microresonators driven by optical pulses, *Nature Photonics* **11**, 600 (2017).
- [58] W. Liang, V. Ilchenko, D. Eliyahu, A. Savchenkov, A. Matsko, D. Seidel, and L. Maleki, Ultralow noise miniature external cavity semiconductor laser, *Nature communications* **6**, 1 (2015).
- [59] K. Goda and B. Jalali, Dispersive Fourier transformation for fast continuous single-shot measurements, *Nature Photonics* **7**, 102 (2013).
- [60] J. K. Jang, M. Erkintalo, S. Coen, and S. G. Murdoch, Temporal tweezing of light through the trapping and manipulation of temporal cavity solitons, *Nature communications* **6**, 1 (2015).
- [61] D. Ceoldo, A. Bendahmane, J. Fatome, G. Millot, T. Hansson, D. Modotto, S. Wabnitz, and B. Kibler, Multiple four-wave mixing and Kerr combs in a bichromatically pumped nonlinear fiber ring cavity, *Optics Letters* **41**, 5462 (2016).
- [62] T. Wildi, V. Brasch, J. Liu, T. J. Kippenberg, and T. Herr, Thermally stable access to microresonator solitons via slow pump modulation, *Optics letters* **44**, 4447 (2019).
- [63] D. V. Strekalov, C. Marquardt, A. B. Matsko, H. G. L. Schwefel, and G. Leuchs, Nonlinear and quantum optics with whispering gallery resonators, *Journal of Optics* **18**, 123002 (2016).
- [64] M. Kues, C. Reimer, J. M. Lukens, W. J. Munro, A. M. Weiner, D. J. Moss, and R. Morandotti, Quantum optical microcombs, *Nature Photonics* **13**, 170 (2019).
- [65] M. Karpov, M. H. P. Pfeiffer, H. Guo, W. Weng, J. Liu, and T. J. Kippenberg, Dynamics of soliton crystals in optical microresonators, *Nature Physics* **15**, 1071 (2019).
- [66] S. Autti, P. J. Heikkinen, J. T. Mäkinen, G. E. Volovik, V. V. Zavjalov, and V. B. Eltsov, AC Josephson effect between two superfluid time crystals, *Nature Materials* **20**, 1 (2020).
- [67] W. Liang, D. Eliyahu, V. S. Ilchenko, A. A. Savchenkov, A. B. Matsko, D. Seidel, and L. Maleki, High spectral purity Kerr frequency comb radio frequency photonic oscillator, *Nature communications* **6**, 1 (2015).
- [68] W. Weng, E. Lucas, G. Lihachev, V. E. Lobanov, H. Guo, M. L. Gorodetsky, and T. J. Kippenberg, Spectral purification of microwave signals with disciplined dissipative Kerr solitons, *Physical Review Letters* **122**, 013902 (2019).
- [69] L. A. Lugiato and R. Lefever, Spatial Dissipative Structures in Passive Optical Systems, *Physical Review Letters* **58**, 10.1103/PhysRevLett.58.2209 (1987).
- [70] H. Keßler, P. Kongkhambut, C. Georges, L. Mathey, J. G. Cosme, and A. Hemmerich, Observation of a Dissipative Time Crystal, *Physical Review Letters* **127**, 043602 (2021).

Acknowledgments. H.T. and A.B.M. acknowledge helpful discussions with W. Liang. The research performed by A.B.M. was carried out at the Jet Propulsion Laboratory, California Institute of Technology, under a contract with the National Aeronautics and Space Administration (80NM0018D0004). K.S. acknowledges support of the National Science Centre, Poland via Project No. 2018/31/B/ST2/00349.

Author contributions. H.T. conceived the idea, initiated and supervised the project, performed the theoretical analysis and numerical modeling, contributed to the design of experiments, and analysed the data. A.B.M. contributed to idea development, numerical simulations, and data analysis, and designed the experiments. L.M. provided resources and managed the experiments. K.S. contributed to conceptualization and data interpretation. H.T. wrote the manuscript with input from all authors. All authors reviewed and approved the final manuscript.

Competing interests. The authors declare no competing financial interests.

Additional information

Supplementary information is available for this paper at URL.

Correspondence and requests for materials should be addressed to H.T.

Supplementary Information for “All-Optical Dissipative Discrete Time Crystals”

Hossein Taheri,¹ Andrey B. Matsko,² Lute Maleki,³ and Krzysztof Sacha⁴

¹*Department of Electrical and Computer Engineering,
University of California Riverside, 3401 Watkins Drive, Riverside, CA 92521*

²*Jet Propulsion Laboratory, California Institute of Technology,
4800 Oak Grove Drive, Pasadena, California 91109-8099, USA*

³*OEwaves Inc., 465 North Halstead Street, Suite 140, Pasadena, CA, 91107, USA*

⁴*Instytut Fizyki Teoretycznej, Uniwersytet Jagielloński,
ulica Profesora Stanisława Łojasiewicza 11, PL-30-348 Kraków, Poland*

This document includes Supplementary Information (SI) to accompany “All-Optical Dissipative Discrete Time Crystals.” Translation symmetry properties of the equations of motion describing a Kerr cavity pumped by a single continuous-wave (CW) laser are reviewed in reference to discrete time crystals (DTCs). It is shown that in a monochromatically pumped resonator, dispersive wave (DW) emission or optical Cherenkov radiation emerging from high-order dispersion (HOD) or avoided mode crossings (AMCs) do not define discrete time translation symmetry (DTTS) in the equations governing microcomb dynamics, thus precluding DTC formation in these systems. We also include more detail on the experimental implementation of the DTCs described in the paper.

I. ABSENCE OF DTTS IN MONOCHROMATICALLY-PUMPED MICROCOMBS

We expound in this section why monochromatically pumped microcombs do not constitute DTCs. This applies also to microcomb soliton trapping observed when certain group velocity dispersion (GVD) profiles (e.g., sign change in the residual dispersion or AMC) create high-power harmonics away from the pump in the comb spectrum. In a driven system, a DTC can arise only when DTTS exists and is broken by a periodic observable whose periodicity is an integer multiple $m > 1$ of that of the drive. In monochromatically pumped DW-emitting solitons and Kerr microcomb soliton crystals, the trapping potential originates from resonator properties (e.g., geometry and dispersion). By inspecting the Lugiato-Lefever equation (LLE) and its germane variants, we show that such effects do not establish any DTTS in the Kerr Hamiltonian, nor in the governing equations of motion. As a corollary, speaking of DTTS breaking in such systems is unjustified.

It should be stressed that when referencing time translation symmetry breaking (TTSB) in monochromatically-pumped microcombs, the observable to base symmetry breaking assessment on is scarcely identified in explicit terms. One can readily show that irrespective of the specific chosen observable, such systems cannot support DTCs. For instance, if photon count at a fixed position is being observed, *continuous* time translation symmetry exists at the input, because the quasi-classical (or coherent) state of the continuous wave (CW) pump laser has Poissonian photon statistics. But then, when a soliton is generated in the output, photon count probability will increase near the soliton peak. As a result, *continuous* TTSB occurs, which clearly does not incorporate DTC formation. If, on the other hand, the response observable is the electric field, then the pump is periodic but the response, strictly speaking, is not (because of the carrier-envelope offset phase) [1–3]. Therefore, the output-over-input periodicity ratio is generally not an integer. This shows that, despite apparent similarities, a soliton or soliton crystal driven by one CW pump does not constitute a DTC.

The rapidly oscillating optical carrier frequency does not enter the LLE [4–7]. It is straightforward to verify that this equation possesses continuous, but not discrete, time translation symmetry. In non-dimensional form and *before* moving to a rotating reference frame, the equation reads

$$\frac{\partial u}{\partial \bar{t}} = \left(-1 + i\alpha + d_1 \frac{\partial}{\partial \theta} + i \frac{d_2}{2} \frac{\partial^2}{\partial \theta^2} - i|u|^2 \right) u + F, \quad (1)$$

where the pump F and spatiotemporal field envelope u are both normalized to the hyperparametric sideband generation threshold and \bar{t} is the slow time normalized to twice the cavity photon lifetime. The normalization follows Ref. [5] and we underscore the use of extra minus signs in normalizing pump-resonance detuning α , free spectral range (FSR) parameter d_1 , and the GVD coefficient d_2 . As in the main text, θ is the azimuthal angle around the circular resonator and related to the fast time τ through $\theta = 2\pi\tau/T_R$, T_R denoting the roundtrip time. It is clear that linear translations with arbitrary increments $\Delta\bar{t}$ and $\Delta\tau$ (equivalently, $\Delta\theta$) of the slow and fast time variables, $\bar{t} \rightarrow \bar{t} + \Delta\bar{t}$ and $\tau \rightarrow \tau + \Delta\tau$ ($\theta \rightarrow \theta + \Delta\theta$), leave Eq. (1) unchanged. Consequently, this equation possesses continuous time

translation symmetry and solutions which fulfill such symmetry are expected. However, owing to the nonlinear term in Eq. (1), symmetry-preserving solutions can be unstable and instead symmetry-broken steady states may emerge. Spontaneous breaking of the continuous time translation symmetry by soliton formation does not amount to DTC generation because there is no DTTS defined by a time-periodic drive which can be violated. It is worth noting that these symmetry properties are maintained in the LLE, which describes the process in a co-rotating reference frame [2, 5].

Without removing the carrier frequency f_P , the excitation term F changes to $F \exp(i2\pi f_P \bar{t})$, which defines a DTTS $\bar{t} \rightarrow \bar{t} + T_P$, in which $T_P = 1/f_P$ is the pump period. However, as noted above, considering the carrier-envelope offset frequency, the electric field of a spontaneously generated soliton is not periodic. In other words, the soliton envelop is periodic with the cavity roundtrip time T_R , but the ratio T_R/T_P is not an integer, because in a monochromatically pumped microcomb soliton train the pulse repetition rate and the pump frequency are fundamentally independent [8]. Moreover, it can be shown that the repetition rate of the pulse train generated with a CW pump always experiences phase diffusion due to quantum noise [9, 10]. Considering the symmetry properties of the equations of motion clarifies why entrainment behavior recently predicted theoretically in certain microcombs [11] and observed experimentally in mode-locked lasers [12] does not amount to DTC formation.

We note that the photon count probability perspective described above has proven to be a valuable one. Recent experiments have explained the timing jitter of soliton microcombs from this viewpoint and shown that, remarkably, the soliton can in essence be considered a particle with the characteristic position-momentum quantum uncertainty between two conjugate variables [9]. Indeed signatures of the quantum nature of solitons have previously been studied extensively in the context of fiber solitons; see, e.g., [13, 14]. From this perspective, the soliton can be considered a massive particle in its ground mechanical quantum state. The large number of photons in this case and the collective effect of photon interactions in the thermodynamic limit notably match the requirements of DTC behavior in Kerr microcombs such that with two-pump excitation, this approach can create DTCs, as we have demonstrated in the main text.

II. ABSENCE OF DTTS IN MICROCOMBS WITH DISPERSIVE WAVES RESULTING FROM HIGHER-ORDER DISPERSION

Resonator residual or integrated dispersion, $D_{\text{int}} = \omega_\eta - (\omega_0 + D_1\eta)$, can predict DW frequencies in the microcomb spectrum. In this expression, $\eta = j - j_0$ is the centered mode number, ω_0 and ω_η signify the frequencies of the pumped mode (j_0) and a generic resonant mode corresponding to mode number j , $D_1/2\pi$ is the FSR at the pump frequency, and $D_2 = \omega_{j_0+1} + \omega_{j_0-1} - 2\omega_{j_0}$ denotes the GVD coefficient. The detuning of resonator modes from the grid defined by microcomb harmonics is minimized in the vicinity of residual dispersion sign change ($D_{\text{int}} = 0$), creating high-power frequency harmonics (DWs) in the spectrum as a result of the optical analogue of Cherenkov radiation [15]. For narrow-band frequency combs and negligibly small third- or higher-order dispersion (HOD), DW emission cannot occur because $D_{\text{int}} = D_2\eta^2/2$ does not cross zero away from the pump. However, in the presence of HOD the residual dispersion, $D_{\text{int}} = D_2\eta^2/2 + D_3\eta^3/6 + \dots$, can vanish for $\eta \neq 0$ to give rise to DWs [16]. The LLE in this case includes higher-order θ -derivatives and takes the following form [17]

$$\frac{\partial u}{\partial \bar{t}} = \left(-1 + i\alpha - \sum_{n=2}^{N>2} i^{n+1} \frac{d_n}{n!} \frac{\partial^n}{\partial \theta^n} - i|u|^2 \right) u + F. \quad (2)$$

Again, Eq. (2) is invariant under linear translations with arbitrary increments $\Delta\bar{t}$ and $\Delta\tau$ of the slow and fast time variables, $\bar{t} \rightarrow \bar{t} + \Delta\bar{t}$ and $\tau \rightarrow \tau + \Delta\tau$. This equation is in the co-moving reference frame, and as noted before, the difference is merely the removal of the $d_1\partial u/\partial\theta$ term such that relevant symmetry properties remain unchanged. Therefore, Eq. (2) possesses continuous time translation symmetry; there is no DTTS and hence DTC formation cannot occur.

III. ABSENCE OF DTTS IN MICROCOMB SOLITON CRYSTALS STABILIZED BY AVOIDED MODE CROSSINGS

The interaction between two mode families with different transverse profiles in a generic resonator is described by two coupled LLEs [18, 19]. The dynamics of microcomb formation when one of the two interacting mode families 1

and 2 is directly pumped (i.e., in a monochromatically-pumped resonator) is captured by

$$\frac{\partial u}{\partial \bar{t}} = \left(-\frac{\bar{\kappa}}{\kappa_2} + i\alpha_1 + \delta_1^{(1)} \frac{\partial}{\partial \theta} + i\frac{d_2^{(1)}}{2} \frac{\partial^2}{\partial \theta^2} - iD^{(1,1)}|u|^2 - iD^{(1,2)}|v|^2 \right) u + F_1, \quad (3)$$

$$\frac{\partial v}{\partial \bar{t}} = \left(-\frac{\bar{\kappa}}{\kappa_1} + i\alpha_2 + \delta_1^{(2)} \frac{\partial}{\partial \theta} + i\frac{d_2^{(2)}}{2} \frac{\partial^2}{\partial \theta^2} - iD^{(2,1)}|u|^2 - iD^{(2,2)}|v|^2 \right) v + F_2, \quad (4)$$

in which $u(\bar{t}, \theta)$ and $v(\bar{t}, \theta)$ are the spatiotemporal field envelopes, respectively, of mode 1 and 2, $\kappa_{1,2}$ is the resonance half width at half maximum (HWHM), $\bar{\kappa} = (\kappa_1 + \kappa_2)/2$ is the average HWHM, $\alpha_{1,2}$ is the detuning, $\delta_1^{(1,2)}$ is the group velocity mismatch of the envelope field with respect to the average group velocity $d_1^{(\text{av})} = (d_1^{(1)} + d_1^{(2)})/2$, $d_1^{(1,2)}$ is the FSR for the respective mode family, $d_2^{(1,2)}$ is the GVD parameter, and $F_{1,2}$ is the effective pump field projected on each of the mode families. For a monochromatic pump tuned primarily to excite one mode family, one of the two drive terms F_1 or F_2 is often negligible; see, e.g., [20]. Coupling between the equations originates from the overlap integrals of the two modes $D^{(j,k)}$, $j, k \in \{1, 2\}$. The notation follows [18]. Like before, \bar{t} is the slow time and the azimuthal angle θ is linearly proportional to the fast time τ .

The set of coupled LLEs in Eq. (3) is invariant under linear translations with arbitrary increments $\Delta\bar{t}$ and $\Delta\tau$ of the slow and fast time variables, i.e., $\bar{t} \rightarrow \bar{t} + \Delta\bar{t}$ and $\tau \rightarrow \tau + \Delta\tau$. Therefore these equations possess continuous time-translation symmetry. In other words, the AMC-induced potential trapping solitons around the resonator does not define DTTS in the equations of motion and so the system cannot give rise to DTCs.

We conclude the discussion on the absence of DTTS in monochromatically-pumped microcombs by highlighting two distinctions offered by second pump exciting subharmonics between the two pumps. Temperature change will shift the modes of a cavity and hence the frequency of the DW or AMC signature in the microcomb power spectrum [21]. As a result, a laser pumping another nearby mode at a fixed frequency or even one pumping the same temperature-shifted mode will in general create a periodic potential with a different periodicity around the cavity. This periodicity is not tied to the pump frequency, and as shown above, does not change the continuous temporal symmetry of the governing equations, nor does it establish any DTTS. In the two-pump system, in contrast, the excitation frequency and the DTTS it defines are always set by the drive, i.e., the beating of the two pumps, so that even with temperature-shifted modes, the same driving frequency can readily be realized. This driving frequency dictates the DTTS of the system, as evidenced by the two panels in Fig. 2 (main text). Additionally, in a singly-pumped microresonator setup with a fixed laser frequency, a microcomb soliton whose span does not cover the spectral position of the more energetic DW harmonic can simply be generated by reducing the pump power and consequently the comb span. In this case, the CW background will not be modulated at all. So, in the same resonator and with the same pump frequency, no periodic potential will form around the resonator, and no soliton trapping and crystallization will occur. In contrast, in the dichromatically-pumped system, DTTS is still present even if the pumps are weak and excite no subharmonics. This is a fundamental distinction, and an essential one, in defining DTCs. It is noteworthy that subharmonic generation in a dual-pump Kerr cavity is possible both in the normal and anomalous dispersion regimes [22–24].

IV. ABSENCE OF STRONG DISPERSIVE WAVE PINNING IN THE EXPERIMENTS

An AMC arises from coupling between different cavity spatial mode families and its signature in the frequency comb spectrum consists of an energetic harmonic. In our experiments, instead of DW-like pinning at a fixed frequency, high-power comb harmonics follow the external pump frequencies in subsequent 2-, 3- and 4-FSR pump separations; see below. Consequently, unlike microcomb soliton crystals whose stability depends on AMCs, subharmonic generation data presented in the main text are not affected by AMCs.

To elaborate, an AMC pins a high-power harmonic in the microcomb spectrum at the position of the mode crossing [25]. While AMCs are practically inevitable in experiments, whether or not they impact the excitation and stability of a microcomb generated in a certain region can partially be judged based on the existence of strong disruptions in the comb teeth pinned in the spectrum and fixed as the pump frequency is shifted. This pinning signature is absent in our experiments, neither when the two pumps generate harmonics through four-wave mixing (FWM), Fig. S1, nor when they excite subharmonics and the beatnote of the pumps is changed in successive FSRs in the same pumping region, Fig. S2. This is particularly manifest in the spectrum for 2-FSR separation of the pumps, Fig. S2(e), which shows no sign of an AMC. Instead, high-power harmonics always follow the external pumps and the FWM harmonics that appear at frequency intervals dictated by their beatnote. Therefore, subharmonic generation in our experiments is not impacted by AMC and mode crossings play no role in stabilizing the observed microcombs. This fact is supported also by our numerical modeling data which demonstrates stable pulse train propagation over hundreds of cavity photon

lifetimes (thousands of drive periods); see Figs. 3(a, d) in the main text. We have not incorporated any AMC or GVD parameter beyond D_2 in our numerical simulations.

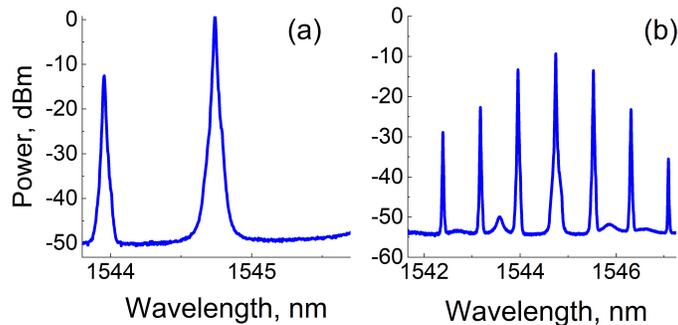


FIG. S1. Experimental data illustrating the two pumps (a) and four-wave mixing creating harmonics spaced by their beatnote (b). Compared to Fig. S2, pump powers are chosen such that subharmonic generation does not occur. No evidence of AMC-induced frequency pinning is observed.

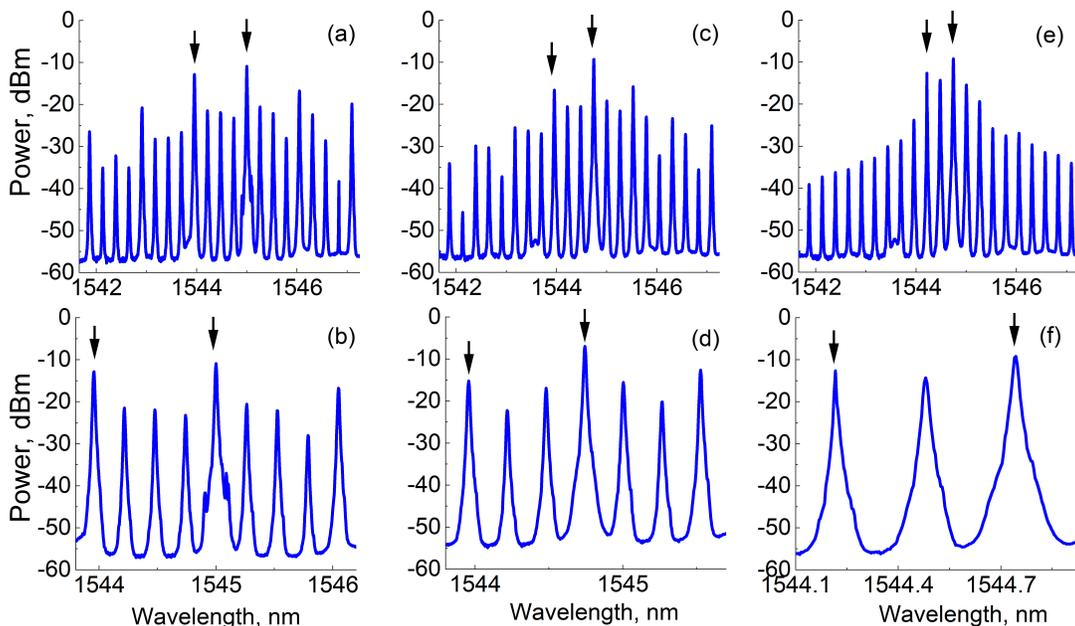


FIG. S2. Experimental data demonstrating stable subharmonic generation for different successively decreased pump beatnotes, (a, b) 4, (c, d) 3, and (e, f) 2 FSRs, in the same pumping region. Each bottom panel is a zoomed-in version of the panel above it. No significant AMC signature or harmonic pinning is observed and high-power microcomb harmonics follow the external pumps. Experimental parameters are the same as those described in the main text (see Methods).

V. SUPPRESSION OF MODE DISRUPTIONS BY THE TWO PUMPS AND THE DESTABILIZING IMPACT OF MODE ANTI-CROSSINGS

We had noted in the main text that our experiments were performed in a regime where none of the pumps could generate solitons independently (see Methods). This is verified in the comb power vs. detuning curve of Fig. S3(a). This figure illustrates that with a single pump, the soliton formation regime is limited to a narrow sliver (the step-like region) and that in experiments we operated to the right of this region, indicated by the red dashed vertical line and arrow, where the pump cannot generate any solitons. Figure S3(b), further discussed below, depicts the same plot as in Fig. S3(a) but with the addition of an AMC near the pumps. System parameters in Figs. S3(a,b) match those of our experiments, with the pump power corresponding to the stronger of the two pumps. The weaker pump, as noted in the

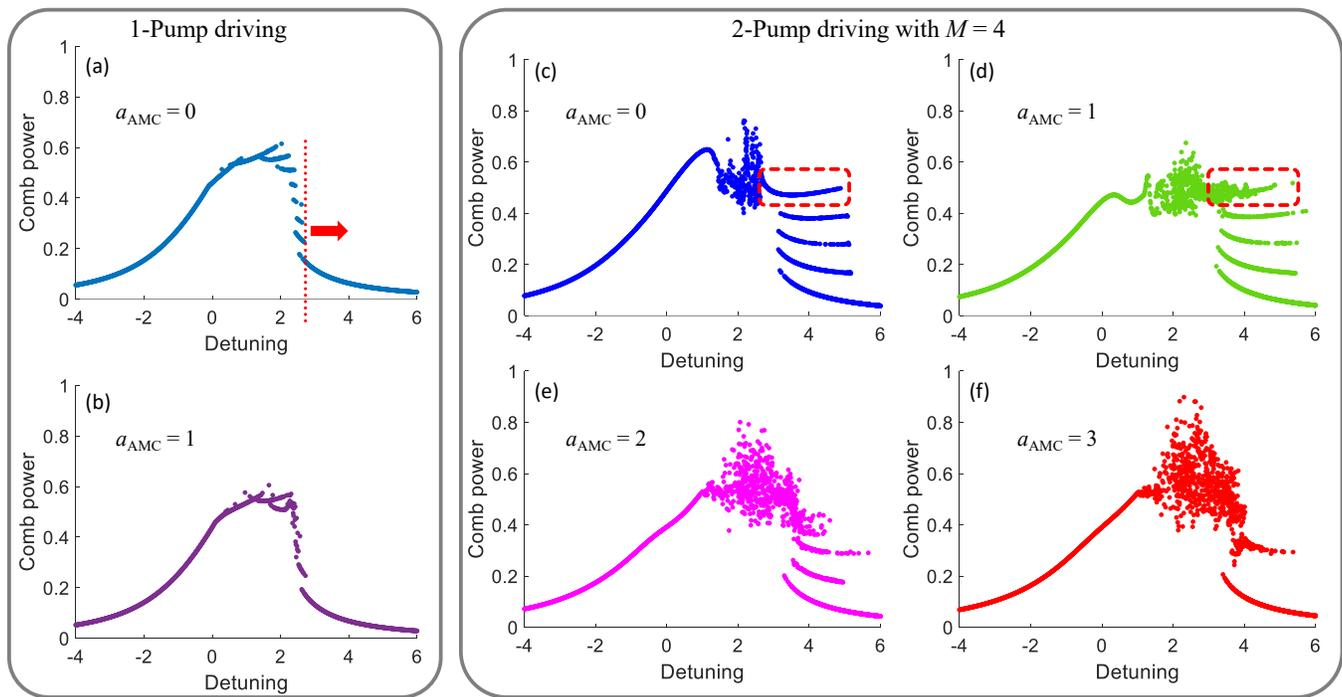


FIG. S3. Investigation of the impact of AMC on subharmonic generation for 4 FSRs between the two pumps. Each curve shows the total comb power vs. detuning at steady state (i.e., each data point on each curve refers to one run till steady state, if existent, was reached). (a, b): Single-pump driving without an AMC (a) and with an AMC parametrized with $a_{\text{AMC}} = 1$ (normalized) and $b = -4$. (b). As noted in the main text (see Methods), the operation region of our system was to the right of the vertical dashed line in (a), where a single pump cannot sustain stable soliton formation. (c-f): Double-pump driving without (c) and with (d-f) the AMC at $b = -4$. In (d-f) the strength of the AMC is increased from $a_{\text{AMC}} = 1$ in (d), to 2 in (e), and 3 in (f). As the AMC grows stronger, it leads to the destabilization of the solitons, evident here as the replacement of clean soliton steps by wider regions where the chaotic power of the unstable microcomb may land after hundreds of cavity lifetimes. An example is highlighted by the boxed regions (dashed red) in (c) and (d), where the top-most step has vanished in (d). In (e) and (f) one and two other high-power steps have vanished as well.

text, is slightly sub-threshold and hence does not obviously support hyperparametric sideband generation or soliton formation. It should be reiterated that, as shown in Sections I and III above, a monochromatically-pumped Kerr cavity, with or without AMC, does not possess discrete time-translation symmetry and hence cannot accommodate DTCs.

Figure S3(c) shows how vastly different the behavior of the system becomes with the addition of the second pump. In this example, the second pump is added 4 FSRs away from the first one ($M = 4$). Instead of 8 very narrow steps in Fig. S3(a), $M + 1 = 5$ wide steps are clearly visible in the figures, as we expected from the theory described in the text. The lower-most step corresponds to no solitons, and the upper ones to 1, 2, 3, and 4 solitons per round-trip time, respectively. All steps are very well-defined with successive runs of the numerical simulation with random initial conditions all resulting in the same steady states with the same comb power at each realization.

In all other panels in Fig. S3, i.e., panels (b, d, e, f), an AMC is added in the numerical simulations. We have used the same model used in Ref. [26] to implement the mode crossing. In this model, the parameter a indicates a measure of the “strength” of the mode crossing and we have represented it with a_{AMC} (normalized to the cavity FWHM) in Fig. S3, while parameter b (non-dimensional) determines its mode number (essentially, frequency). In panels (b, d-f) of Fig. S3, $b = -4$. (Note that all of our experimental data are reported vs. wavelength, not frequency.) Without a second pump and with $a_{\text{AMC}} = 1$, Fig. S3(b), some of the steps in the narrow soliton formation region of Fig. S3(a) show clear signs of destabilization. This observation matches findings previously reported in the literature, particularly that AMCs very close to the pump destabilize microcombs and hinder soliton formation; see, e.g., [26].

In Figs. S3(d, e, f), a_{AMC} is increasing from 1 to 3, respectively. With two-pump driving and the small value of $a_{\text{AMC}} = 1$, even though the lower-level stairs do not change much, destabilization of the solitons starts to occur noticeably. The destruction of stable soliton steps is especially clear from the top-most step (boxed with a red dashed-line rectangle) and would translate into large phase noise for the subharmonic beatnote. Figures S3(e, f), where $a_{\text{AMC}} = 2$ and 3, demonstrate how by increasing the strength of the AMC, soliton steps are almost completely

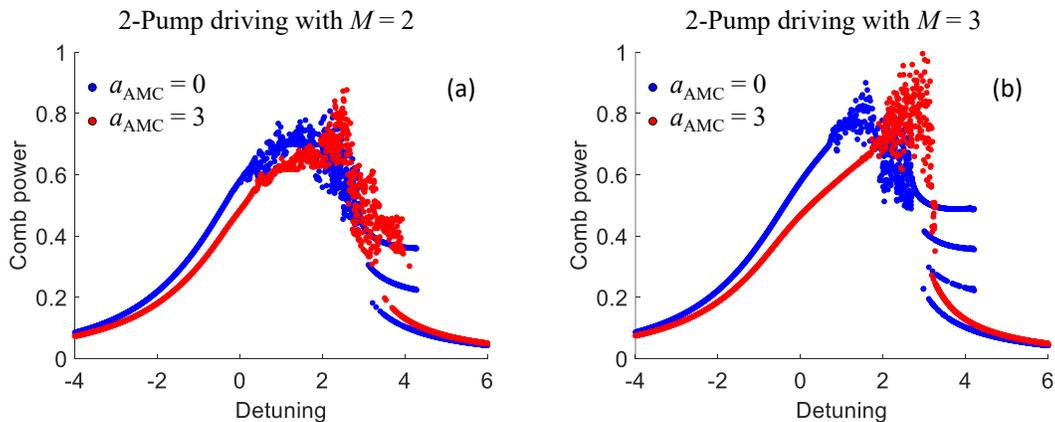


FIG. S4. Investigation of the impact of AMC on subharmonic generation, similar to Fig. S3, but for 2 (a) and 3 (b) FSRs between the two pumps.

washed away, leaving only the bottom step (no solitons) and a fuzzy trace of the destabilized third step in panel (f). The trend is clear: further increase of the AMC strength would completely eradicate soliton steps. It is worth noting that with smaller a_{AMC} (e.g., $a_{\text{AMC}} = 0.5$) the differences with the AMC-free case were unremarkable, indicating that the AMC is completely subjugated by the cooperation of the two pumps, as if the mode disruptions did not exist at all. It should be emphasized that the same destabilizing effect of AMCs is observed (and is even more severe) for the same AMC frequency and with $M = 2$ and 3, as the overlaid plots in Fig. S4 show. (Not included herein, we have observed the same disruptive influence of AMCs at other values of b as well, e.g., for the AMC 5 FSRs away from the stronger pump, $b = -5$.)

The results discussed above show that AMCs, especially those so close to the pumps, would only hurt, and not assist, subharmonic generation. In other words, the existence of AMCs would hinder the emergence of the stable and low phase noise subharmonics that herald DTC formation. In our experiments, we have observed stable microcombs with robust subharmonics in all of the discussed cases ($M = 2, 3$, and 4), which would not have been possible if the AMCs were dominant. This observation confirms that AMCs in our experiments were indeed weak and completely overshadowed by the pumps.

-
- [1] S. T. Cundiff, Phase stabilization of ultrashort optical pulses, *Journal of Physics D: Applied Physics* **35**, R43 (2002).
 - [2] A. Kovach, D. Chen, J. He, H. Choi, A. H. Dogan, M. Ghasemkhani, H. Taheri, and A. M. Armani, Emerging material systems for integrated optical Kerr frequency combs, *Adv. Opt. Photon.* **12**, 135 (2020).
 - [3] H. Taheri and A. B. Matsko, Dually-pumped Kerr microcombs for spectrally pure radio frequency signal generation and time-keeping, in *Laser Resonators, Microresonators, and Beam Control XXI*, Vol. 10904 (International Society for Optics and Photonics, 2019) p. 109040P.
 - [4] Y. Chembo and N. Yu, Modal expansion approach to optical-frequency-comb generation with monolithic whispering-gallery-mode resonators, *Phys. Rev. A* **82**, 033801 (2010).
 - [5] Y. Chembo and C. Menyuk, Spatiotemporal Lugiato-Lefever formalism for Kerr-comb generation in whispering-gallery-mode resonators, *Phys. Rev. A* **87**, 053852 (2013).
 - [6] A. Matsko, A. Savchenkov, W. Liang, V. Ilchenko, D. Seidel, and L. Maleki, Mode-locked Kerr frequency combs, *Opt. Lett.* **36**, 2845 (2011).
 - [7] S. Coen, H. Randle, T. Sylvestre, and M. Erkintalo, Modeling of octave-spanning Kerr frequency combs using a generalized mean-field Lugiato-Lefever model, *Opt. Lett.* **38**, 37 (2013).
 - [8] A. B. Matsko and L. Maleki, On timing jitter of mode locked Kerr frequency combs, *Optics Express* **21**, 28862 (2013).
 - [9] C. Bao, M.-G. Suh, B. Shen, K. Şafak, A. Dai, H. Wang, L. Wu, Z. Yuan, Q.-F. Yang, A. B. Matsko, F. K. Kärtner, and K. J. Vahala, Quantum diffusion of microcavity solitons, *Nature Physics* **17**, 462 (2021).
 - [10] A. B. Matsko and L. Maleki, Noise conversion in Kerr comb RF photonic oscillators, *JOSA B* **32**, 232 (2015).
 - [11] D. C. Cole and S. B. Papp, Subharmonic Entrainment of Kerr Breather Solitons, *Physical Review Letters* **123**, 173904 (2019).
 - [12] T. Xian, L. Zhan, W. Wang, and W. Zhang, Subharmonic Entrainment Breather Solitons in Ultrafast Lasers, *Physical Review Letters* **125**, 163901 (2020).
 - [13] L. A. Lugiato and F. Castelli, Quantum noise reduction in a spatial dissipative structure, *Physical Review Letters* **68**,

- 10.1103/PhysRevLett.68.3284 (1992).
- [14] P. D. Drummond, R. M. Shelby, S. R. Friberg, and Y. Yamamoto, Quantum solitons in optical fibres, *Nature* **365**, 307 (1993).
 - [15] V. Brasch, M. Geiselmann, T. Herr, G. Lihachev, M. H. P. Pfeiffer, M. L. Gorodetsky, and T. J. Kippenberg, Photonic chip-based optical frequency comb using soliton Cherenkov radiation, *Science* **351**, 357 (2016).
 - [16] C. Bao, H. Taheri, L. Zhang, A. Matsko, Y. Yan, P. Liao, L. Maleki, and A. Willner, High-order dispersion in Kerr comb oscillators, *JOSA B* **34**, 715 (2017).
 - [17] M. Lamont, Y. Okawachi, and A. Gaeta, Route to stabilized ultrabroadband microresonator-based frequency combs, *Opt. Lett.* **38**, 3478 (2013).
 - [18] G. D'Aguanno and C. R. Menyuk, Nonlinear mode coupling in whispering-gallery-mode resonators, *Physical Review A* **93**, 043820 (2016).
 - [19] M. Karpov, M. H. P. Pfeiffer, H. Guo, W. Weng, J. Liu, and T. J. Kippenberg, Dynamics of soliton crystals in optical microresonators, *Nature Physics* **15**, 1071 (2019).
 - [20] A. Matsko, W. Liang, A. Savchenkov, D. Eliyahu, and L. Maleki, Optical Cherenkov radiation in overmoded microresonators, *Optics Letters* **41**, 2907 (2016).
 - [21] Y. Wang, F. Leo, J. Fatome, M. Erkintalo, S. G. Murdoch, and S. Coen, Universal mechanism for the binding of temporal cavity solitons, *Optica* **4**, 855 (2017).
 - [22] T. Hansson and S. Wabnitz, Bichromatically pumped microresonator frequency combs, *Phys. Rev. A* **90**, 013811 (2014).
 - [23] Y. Okawachi, M. Yu, K. Luke, D. O. Carvalho, S. Ramelow, A. Farsi, M. Lipson, and A. L. Gaeta, Dual-pumped degenerate Kerr oscillator in a silicon nitride microresonator, *Optics Letters* **40**, 5267 (2015).
 - [24] H. Taheri and A. Matsko, Crystallizing Kerr Cavity Pulse Peaks in a Timing Lattice, in *Frontiers in Optics + Laser Science APS/DLS (2019), paper JTU3A.90* (Optical Society of America, 2019).
 - [25] X. Xue, M. Qi, and A. M. Weiner, Normal-dispersion microresonator Kerr frequency combs, *Nanophotonics* **5**, 244 (2016).
 - [26] T. Herr, V. Brasch, J. D. Jost, I. Mirgorodskiy, G. Lihachev, M. L. Gorodetsky, and T. J. Kippenberg, Mode spectrum and temporal soliton formation in optical microresonators, *Phys. Rev. Lett.* **113**, 123901 (2014).